RSC Advances

PAPER

View Article Online
View Journal | View Issue

Cite this: *RSC Adv.*, 2023, **13**, 9208

Design of a new method for one-pot synthesis of 2-amino thiazoles using trichloroisocyanuric acid in the presence of a novel multi-functional and magnetically catalytic nanosystem: Ca/4-MePy-IL@ZY-Fe_3O_4†

Mehdi Kalhor, * Zahra Vahedi and Hanieh Gharoubi

In this study, an effective approach was developed to synthesize a novel, multifunctional ionic liquid nanocatalyst based on zeolite-Y with 4-methylpyridinium chloride (4-MePy-Cl) and calcium ions (Ca/4-MePy-IL@ZY). Then, Fe_3O_4 nanoparticles were produced inside the zeolite pores with the use of ultrasonic waves. XRD, FESEM, FT-IR, EDX-Map, TGA-DTA, VSM, BET, and atomic absorption techniques were used to identify the structure of the magnetic nanocomposite. Then, its catalytic activity in the one-pot synthesis of 2-aminothiazoles using trichloroisocyanuric acid (TCCA) as a green supplier of halogen ions for intermediates was studied. To provide ideal conditions for the preparation of pure products, first, the one-pot reaction of acetophenone and thiourea in various solvents, different temperatures, and the presence of different amounts of nanocatalysts and the molar amount of TCCA was used. Next, the reaction was investigated in the one-pot preparation of 2-aminothiazole derivatives under optimal conditions. This method replaces iodine (I_2), a toxic reagent, for the first time with TCCA, a safe and sustainable source of halogen. The use of non-toxic solvent and a cheap, safe, recyclable nanocatalyst, quick reaction times, high efficiency, and ease of nanocatalyst separation with the aid of a magnet are additional benefits of this method. This has led to this procedure being classified as "green chemistry".

Received 4th February 2023
Accepted 16th March 2023

DOI: 10.1039/d3ra00758h

rsc.li/rsc-advances

1. Introduction

One of the major components in a number of natural compounds is thiazole and its derivatives. As a member of the thiazole group, 2-aminothiazole plays an important role in synthetic and medicinal chemistry.[1,2] A large variety of natural substances, medications, and agrochemicals have the aminothiazole framework. It is also found in substances with a variety of significant biological and pharmacological qualities.[3,4] There are several methods for synthesizing this class of chemicals (Fig. 1). The approaches shown in Fig. 1 each have advantages and disadvantages, but it appears that the approach utilizing methyl carbonyl (α-halo ketones) and thiourea as precursors is the most practical (Hantzsch condensation).[5,6] Since active methylene ketones can be *in situ* α-halogenated, modified Hantzsch (one-pot) condensation of active methylene ketones with thioureas has received much attention in order to save time and costs in the synthesis of thiazoles. In this regard, *in situ* α-halogenation strategies using various halogenating reagents including Br_2,[7] I_2,[8–11] NBS,[12,13] 1,3-dichloro 5,5-dimethylhydantoin,[14] *etc.*[15,16] have been developed. Despite the benefits of the earlier techniques, there is still a need to enhance the preparation of 2-aminothiazoles using novel techniques and catalysts since the class of these compounds has a large impact on synthetic chemistry and medicines.

In this regard, *N*-halo reagent-based pot-economy techniques are widely used for the synthesis of heterocycles. Trihaloisocyanuric acids, one of the *N*-halo reagents, are efficient and stable electrophilic halogenating reagents that are commercially available or prepared from readily accessible materials. They may incorporate halogen atoms into organic compounds without the use of hazardous and corrosive X_2. They are also capable of transferring up to three halogen atoms to a substrate, and in reactions involving trihaloisocyanuric acids, the cyanuric acid (CA) by-product can be recycled to make more trihaloisocyanuric acid.[17,18] In a variety of processes, all of these compounds have been demonstrated to be highly effective halenium (X^+) releasing agents, resulting in good to outstanding yields of the appropriate halogenated products under green conditions. Therefore, a variety of products, such

Department of Chemistry, Payame Noor University, Tehran, 19395-4697, Iran. E-mail: mekalhor@pnu.ac.ir; mekalhor@gmail.com; Fax: +98 2537179170; Tel: +98 2537179170

† Electronic supplementary information (ESI) available. See DOI: https://doi.org/10.1039/d3ra00758h

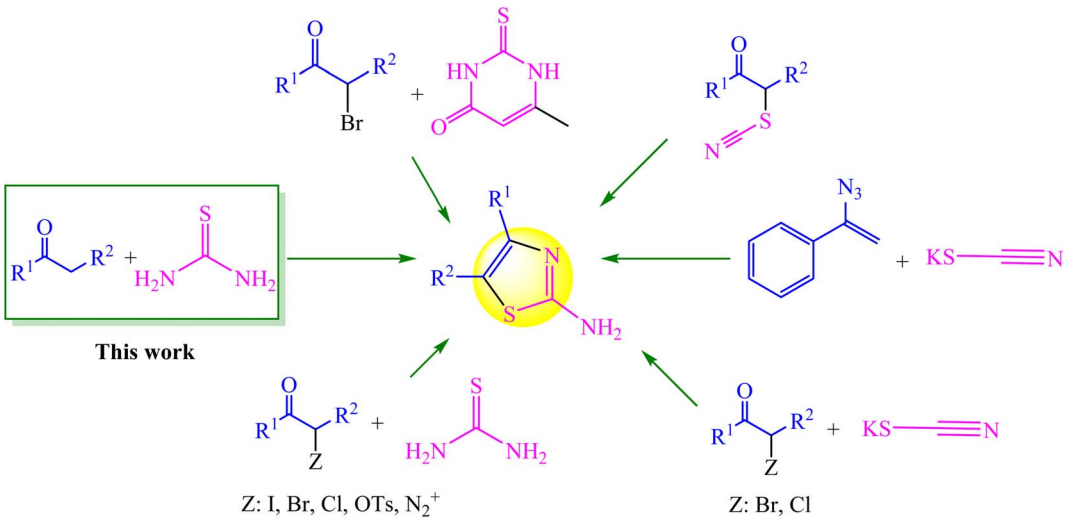

Fig. 1 Various methods for the synthesis of 2-aminothiazoles.

as haloarenes, halohydrins, halocarbonyls, *etc.* can be produced depending on the kind of nucleophile interacting with these electrophilic agents.[19,20] The most frequently used haloisocyanuric acid is trichloroisocyanuric acid (TCCA), which is a stable solid, is also used for synthesis of aryl and heteroaryl tetrafluoro-λ6-sulfanyl chlorides and commercially to sterilize swimming pools.[21] However, to the best of our knowledge, trichloroisocyanuric acid (TCCA) has not been used as a halogenated green reagent for the synthesis of 2-aminothiazoles.

Zeolites as porous crystalline aluminosilicates have recently emerged as a significant class of high-tech materials for immobilization catalysts due to their high surface area, nanoporous crystalline structure, high thermostability, persistence in all organic solvents, lack of waste or disposal issues, ability to conduct cation exchange and safety in addition to many other industrial and environmental benefits.[22–24] Zeolite–NaY has been a source of significant issues in fluid catalytic cracking (FCC) and gasoline production because of its significant acidity, great hydrothermal stability, and low price. Recent times have seen the usage of zeolite–NaY as the best support for heterogeneous catalysts.[25] In zeolites, in addition to metal ion exchange processes, existing hydroxy groups can also play an important role in the fabrication and invention of novel multifunctional catalysts by fusing organic catalysts into their structural compositions.[26]

One of the primary goals of green chemistry is to reduce the damage caused by the use of hazardous chemicals, and the synthesis of novel multi-functional catalysts has recently attracted a lot of attention. As a result, the creation and manufacturing of heterogeneous nanocatalysts, particularly those with several functions, is a popular topic of study today. In multi-step processes requiring the same or distinct active sites in a single pot, multi-functional nanocatalysts are useful.[27–29] Additionally, the preparation of catalysts at the nanoparticle scale can also be extremely successful in their catalytic activity due to the large surface area to volume ratio. Zeolite-Y and metal/zeolite-Y have been employed as the best supports for bifunctional nanocatalysts, organic and heterocyclic chemicals, and ionic liquids.[30–32] The immobilization of ionic liquids as a type of liquid substance with unique properties on zeolite supports *via* covalent bonds is efficiently used in catalytic processes.[33,34]

Magnetic separations, with no filtration or centrifugation involved have recently been developed as an optional method for recovering and reusing heterogeneous catalysts. Due to its remarkable magnetic, physical, surface chemical, and catalytic properties, great stability, and simplicity of recovery with an external magnet, iron oxide magnetic nanoparticles (Fe_3O_4-NPs) have attracted attention in recent years.[35,36]

In view of the aforesaid facts, we describe the synthesis and characterization of Ca/4-MePy-IL@ZY-Fe_3O_4 nanoporous, a recoverable, magnetically and multifunctional nanocatalyst for the quick and simple synthesis of 2-aminothiazoles using methyl ketones and thiourea as precursors and TCCA as a green source of halogen ions at 80 °C in EtOH solvent (Scheme 1).

2. Experimental

2.1. Synthesis of Ca/4-MePy-IL@ZY

1.0 g of zeolite–NaY with 1.5 mmol of calcium chloride (0.220 g) was stirred for 20 h at room temperature and then the solid of Ca@zeolite–Y centrifuged and after dispersed for three times, washed with water and dried at 50 to 60 °C. Next, 1.0 g of Ca@zeolite–Y and 0.5 mL of 3-chloropropyltriethoxysilane ($(EtO)_3Si$–PrCl) were stirred and refluxed for 24 h in 20 mL of toluene. In the following, the water–ethanol mixture and the resulting precipitate were placed in an ultrasonic bath three times for 10 min, centrifuged for 50 min, and after washing with water, dried in an oven. Finally, in 20 mL of toluene, 0.25 mmol of 4-methylpyridine was added to Ca/PrCl@zeolite–Y (1.0 g) and the resulting mixture was refluxed for 24 h. As in the previous step, the resulting mixture was centrifuged three times, placed

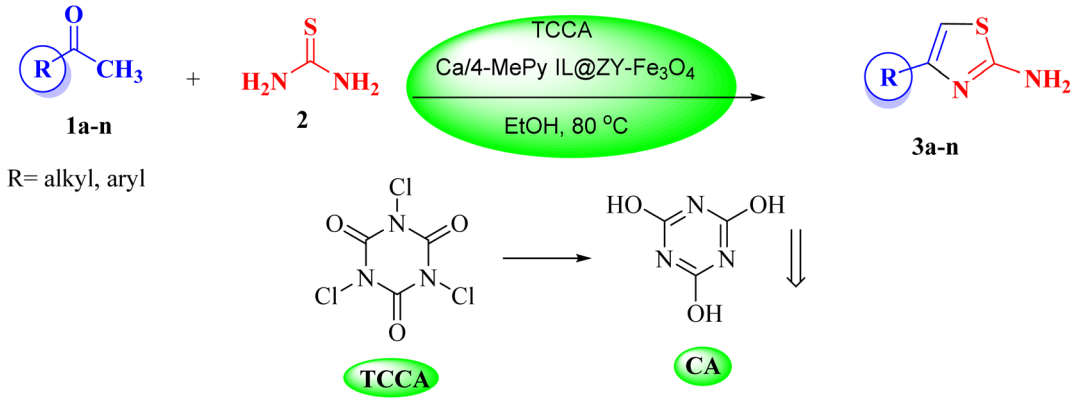

Scheme 1 The synthetic pathway of 2-aminothiazoles using Ca/4-MePy-IL@ZY-Fe_3O_4.

in an ultrasonic bath and washed with water to preserve the structure of the nanocomposite, and finally dried at 70 °C for 2 hours.

2.2. Synthesis of Ca/4-MePy-IL@ZY-Fe_3O_4

In order to prepare the final magnetic nanocatalyst, 1.0 g of the nanocomposite prepared in the previous step was dispersed in distilled water (50 mL). Next, at 60 °C, 1.0 mmol of $FeCl_2 \cdot 4H_2O$ and 2.0 mmol of $FeCl_3 \cdot 6H_2O$ was added to the aforesaid solution and mixed. Then, under a nitrogen atmosphere, 25% ammonia solution was added drop by drop while stirring, and after 30 min, with the start of the reaction and the production of Fe_3O_4 nanoparticles, the color of the brown solution became dark and it was ready at the same time and loaded into the zeolite cavities. Finally, the black solids were separated from the mixture using an external magnet, which was then washed with water and dried in an oven for 5 h (Scheme 2).

2.3. Catalytic synthesis of 2-aminothiazole derivatives

In 3.0 mL of EtOH, 0.5 mmol TCCA, 1.5 mmol acetophenone derivative, and 0.01 g of Ca/4-MePy-IL@ZY-Fe_3O_4 were stirred at 80 °C for 25 min. The completion of the reaction was monitored by TLC and after confirming the production of the intermediate product carbonyl alkyl halide, 1.0 mmol of thiourea was added to the reaction mixture. After the completion of the reaction within the appropriate time mentioned in Table 3, the nanocatalyst was then gathered utilizing an external magnet. To produce a neutral solution, 10% sodium bicarbonate solution is then added to the mixture. In this situation, filter paper should be used to separate thiazole precipitate. By washing the

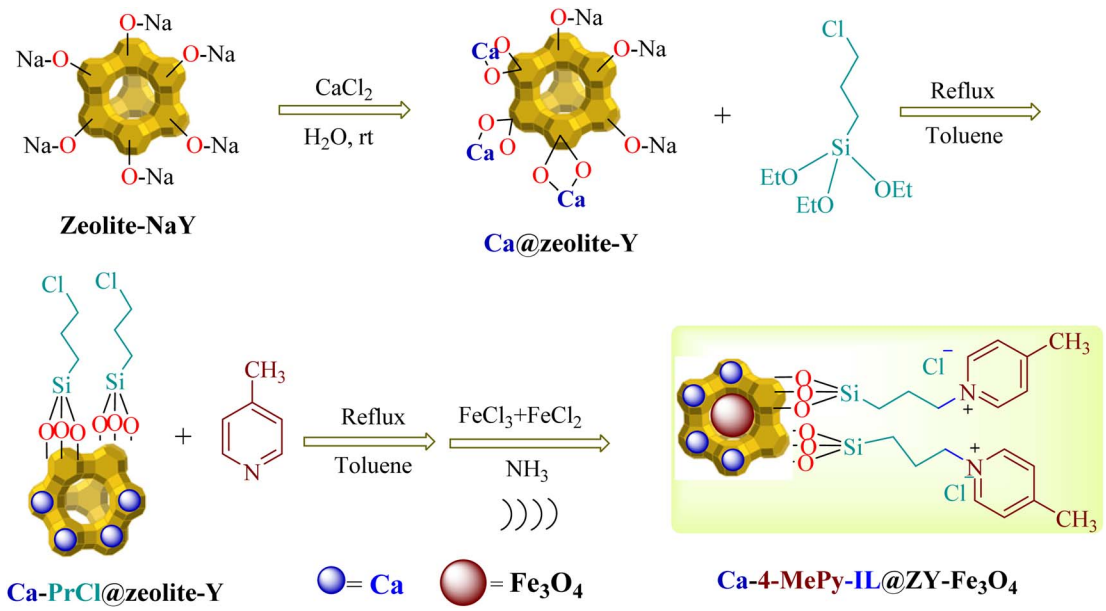

Scheme 2 The procedure for the synthesis of Ca/4-MePy-IL@ZY-Fe_3O_4 nanocomposite.

precipitate with water and ethanol and drying in an oven, the pure product of substituted 2-aminothiazole is obtained. The side product of cyanuric acid is produced by adding a few drops of diluted acid and neutralizing the solution under the filter. All 2-aminothiazole products are known and were identified by comparison of their melting point, FT-IR and ^{1}H NMR with those of authentic samples.

2.4. Identification of some of 2-aminothiazole derivatives

2.4.1. 4-(Pyridin-2-yl)thiazol-2-amine (3j). FT-IR (KBr), υ_{max} 3429 (NH_2), 1635 (C=N), 1234, 1145 (C=C), 1057, 1014 (C–N), 884 (S–C=N), 851, 578 cm^{-1}; ^{1}H NMR (500 MHz, DMSO-d_6): δ_H 8.89 (s, 1H, H-pyridyl), 8.52 (d br, 1H, H-pyridyl), 8.05 (d, J = 7.20 Hz, 1H, H-pyridyl), 7.63 (s, 1H, H-pyridyl), 7.46 (s, 2H, NH_2), 7.35 (s, 1H, H-thiazole) ppm.

2.4.2. 4-(Pyridin-4-yl)thiazol-2-amine (3l). FT-IR (KBr), υ_{max}: 3428 (NH_2), 1633, 1612 (C=N), 1580, 1340, 1291 (C=C), 1025 (C–N), 811 (S–C=N), 703 cm^{-1}; ^{1}H NMR (500 MHz, DMSO-d_6): δ_H 8.90 (s, 1H, H-pyridyl), 8.52 (d br, 1H, H-pyridyl), 7.89 (d, J = 7.20 Hz, 1H, H-pyridyl), 7.63 (s, 1H, H-pyridyl), 7.46–7.31 (t br, 3H, NH_2 and H-thiazole) ppm.

2.4.3. 2-Amino-5,5-dimethyl-5,6-dihydrobenzo[*d*]thiazol-7(4*H*)-one (3m). FT-IR (KBr), υ_{max}: 3390, 3297, 3100 (NH_2), 2958 (C–H), 1644 (C=O), 1625, 1600 (C=N), 1511, 1369, 1311, 1255, (C=C) 1146, 1055 (C–N), 584 (S–C=N) cm^{-1}; ^{1}H NMR (500 MHz, DMSO-d_6): δ_H 8.09 (s, 2H, NH_2), 2.58 (s, 2H, CH_2), 2.26 (s, 2H, CH_2), 1.03 (s, 3H, CH_3), 1.02 (s, 3H, CH_3) ppm; ^{13}C NMR (125 MHz, DMSO-d_6): δ_C 189.3 (C=O), 174.2 (C=N), 166.9, 117.4, 51.2, 40.9, 34.2, 28.4 ppm.

3. Results and discussion

3.1. Catalyst characterization

According to Scheme 2, Ca/4-MePy-IL@ZY-Fe_3O_4 was produced. Ca/PrCl@zeolite–Y nanocomposites were produced by first modifying the Ca@zeolite–Y with ($(EtO)_3$Si-PrCl). The subsequent reaction between 4-methylpyridine (4-MePy) and Ca/Pr–Cl@zeolite–Y produced the ionic liquid with zeolite-supported 4-Me pyridinium cation. Ionic liquid and Ca@zeolite together create a multi-functional nanocatalyst that is more efficient than any component alone because each component of the catalyst increases its efficacy. Finally, the magnetic nanoparticles were stabilized under sonication inside the functionalized zeolite pores to form the target magnetic nano-system. Next, the new magnetic nanohybrid were characterized using FT-IR, XRD, EDX, BET, TGA/DTA, FESEM, VSM and the elemental mapping.

The FT-IR spectra of zeolitic nanoporous are shown in Fig. 2. The zeolite–NaY spectrum in Fig. 2a reveals that the vibration bands at 3459 cm^{-1} and 1635 cm^{-1} are connected to the O–H stretching of hydrogen-bonded internal silanol groups and the bending vibration of adsorbed water, respectively. The symmetric and asymmetric stretching vibrations of the Si–O–Si groups are represented by the strong absorption at 1021 cm^{-1} and the weak absorption at 792 cm^{-1}, respectively. Because

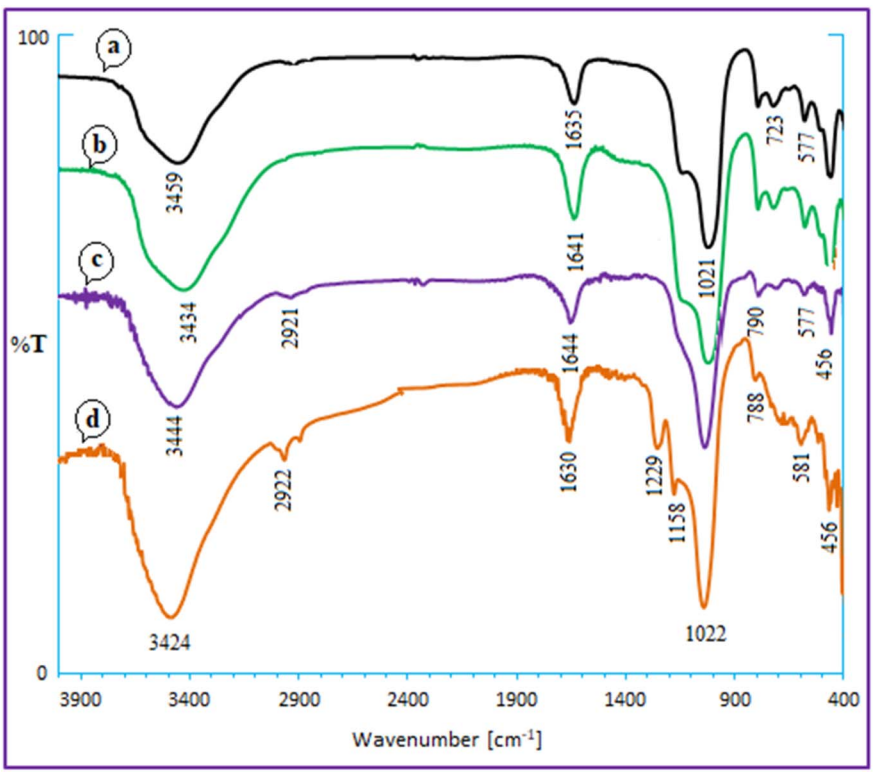

Fig. 2 FT-IR spectra for zeolite–NaY (a), Ca–ZY (b), Ca/4-MePy-IL@ZY (c) and Ca/4-MePy-IL@ZY-Fe_3O_4 (d).

there are not many functional groups in the structure of the zeolite, the other spectra in Fig. 2b–d are not significantly different from the spectrum of zeolite–NaY. In addition, the absorption band appearing in the region of 581 cm^{-1} in Fig. 2d shows the stretching vibrations of the Fe–O bond. The presence of this signal and the red or blue shift of some signals compared to Fig. 2d confirm the magnetization of the nanocomposite structure.

The morphology of zeolite–NaY, Ca–zeolite-Y, and Ca/4-MePy-IL@ZY-Fe_3O_4 nanocomposites was investigated by FE-SEM, and the corresponding results are in Fig. 3. The catalyst is depicted in these images as sheet-shaped particles with small, medium, and large polyhedral cavities. Additionally, it shows that the morphology of the structure was conserved and that there was little change in the general shape of the primary zeolite's distinctive structure during the functionalization process and the nano-cavities sizes are in the 11–15 nm range, which confirms the crystalline and nanostructure of the desired mesoporous. Analysing the statistical diagram of particle size distribution or the diameter of holes distributed on the surface of the nanocatalyst (histogram), it was found that most of the particle sizes are in the range of 15–20 nm and the majority of the holes are in the range of 10–30 nm which is typical of mesoporous materials (Fig. 4).

EDX-Map analysis was used to determine the chemical composition of Ca/4-MePy-IL@ZY-Fe_3O_4 (Fig. 5). As shown in Fig. 5 confirmed that C, O, N, Fe, Ca, Na, Cl and Si were the main components in Ca/4-MePy-IL@ZY-Fe_3O_4. Also, looking at the table of the qualitative results and determining the ratio of Si to Al (Si/Al = 3.04) and comparing with fresh zeolite-Y (Si/Al = 2.78), it was found that the structure of zeolite-Y is still preserved in the functionalization process.

The catalyst crystal structure of zeolite–NaY, Ca/4-MePy-IL@ZY and Ca/4-MePy-IL@ZY-Fe_3O_4 were investigated *via* XRD analysis (Fig. 6). According to Fig. 6, the prominent peaks at 2θ values of 6.1° (111), 10.0° (220), 11.7° (311), 15.6° (222), 18.6° (440), 20.3° (551), 23.6° (553), 26.9° (642), 30.7° (822), 31.3° (555) and 34.0° (840) indicate the presence of zeolite–NaY (JCPDS 39-1380).[37] This result indicates that the framework of the zeolite–NaY was not damaged after modification (Fig. 6b). Additionally,

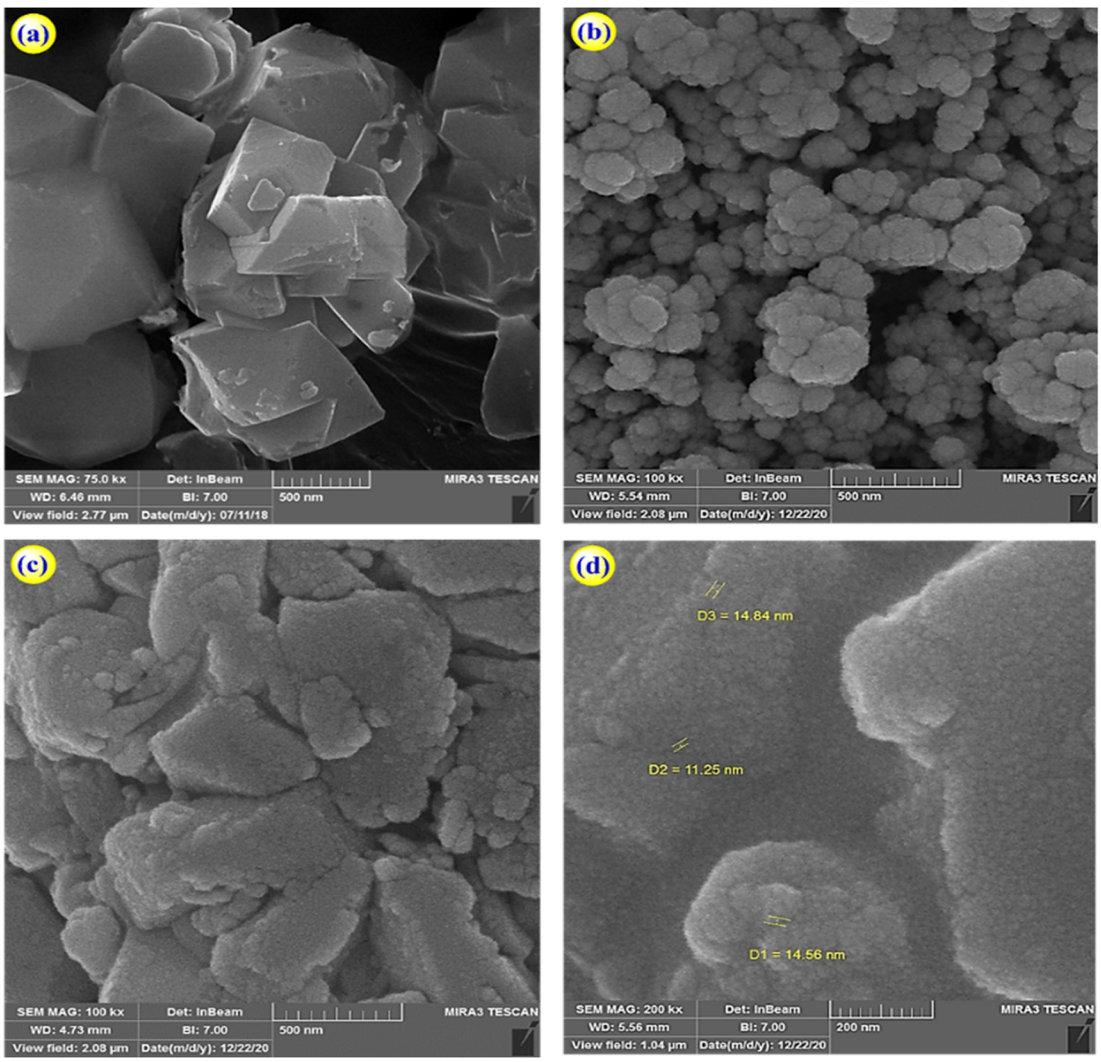

Fig. 3 FE-SEM images of zeolite–NaY (a), Ca@ZY (b) and Ca/4-MePy-IL@ZY-Fe_3O_4 (c and d).

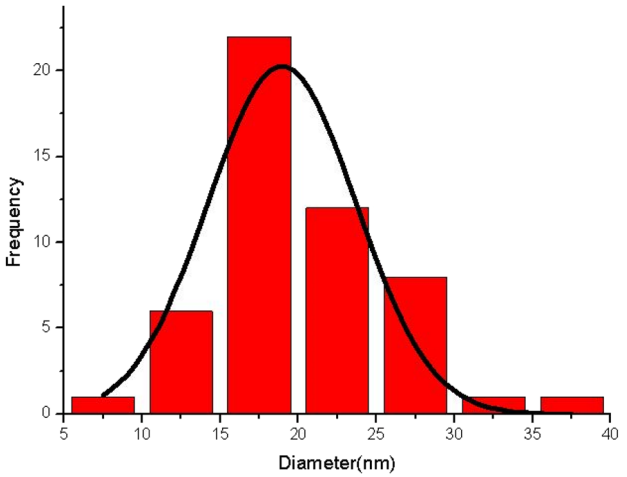

Fig. 4 Histogram of particle size distribution in Ca/4-MePy-IL@ZY-Fe_3O_4 nanocatalyst.

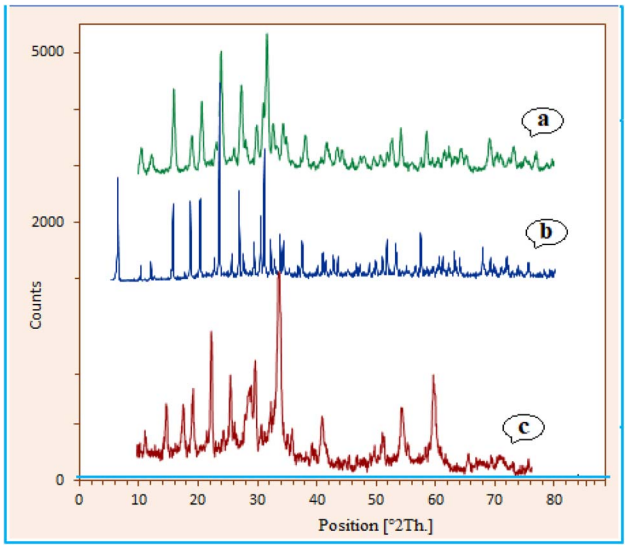

Fig. 6 XRD spectrum of zeolite–NaY (a), Ca/4-MePy-IL@ZY (b) and Ca/4-MePy-IL@ZY-Fe_3O_4 (c) nanoporous.

as shown in Fig. 6c, significantly new peaks were found 2θ values of 30.4 (220), 35.6 (311), 43.2 (400), 54.2 (422), 57.4 (511) and 62.8 (440), which are equal to cubic Fe_3O_4 (JCPDS 19-0629).[38]

As shown in Fig. 7, VSM analysis was used to evaluate the magnetic properties of Ca/4-MePy-IL@ZY-Fe_3O_4. The analyses show 15 emu g^{-1} saturation magnetization for Ca/4-MePy-

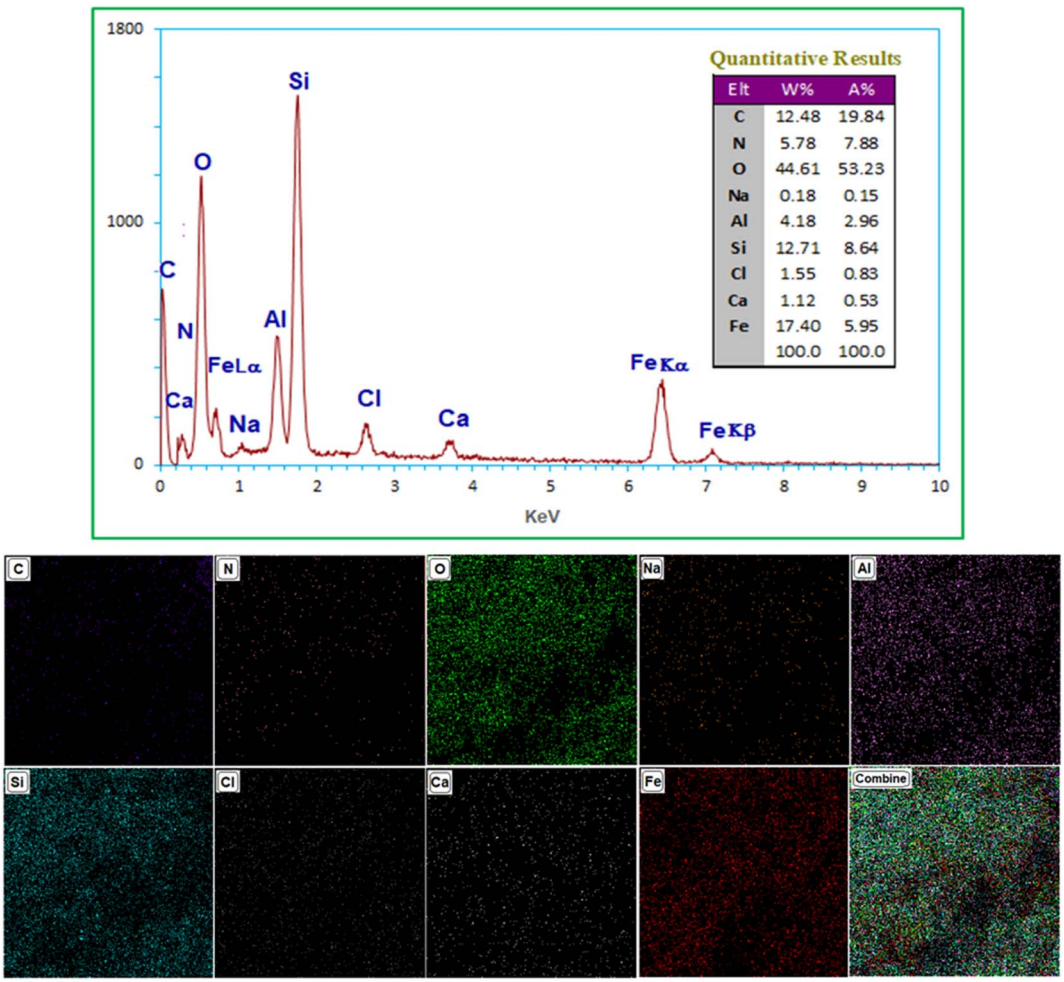

Fig. 5 The EDX-Map diagram of representative elements in Ca/4-MePy-IL@ZY-Fe_3O_4.

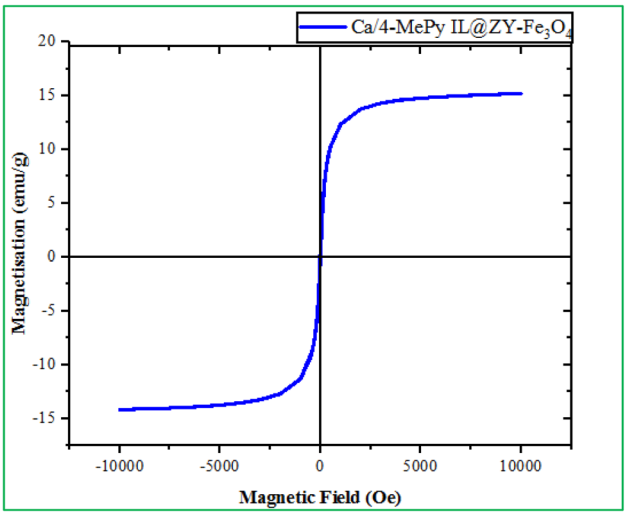

Fig. 7 Field-dependent magnetization curve measured at room temperature for Ca/4-MePy-IL@ZY-Fe_3O_4.

IL@ZY-Fe_3O_4, respectively. As a consequence, the catalyst may be easily retrieved and separated using an external magnet.

The catalyst thermal stability was examined using TGA-DTG. In the study carried out in 37–700 °C range, the weight loss of Ca/4-MePy-IL@ZY-Fe_3O_4 was amply confirmed (Fig. 8). The sample's weight loss in 120–200 °C is caused by the release of water or organic solvents from the structure. The decomposition of organic species is related to the second weight in the range of 200–400 °C. As a result, organic groups have functionalized the surface of zeolite–NaY. The elimination of calcium ions and the altered magnetic-zeolite structure may be responsible for the ultimate weight loss in the 450–650 °C temperature range.

The textural and structural characteristics of zeolitic nanostructures are assessed using N_2 adsorption–desorption isotherm measurements. Fig. 9a depicts the N_2 adsorption–desorption isotherms for the zeolite–NaY and Ca@zeolite-Y. These samples demonstrate type I isotherms, which show the

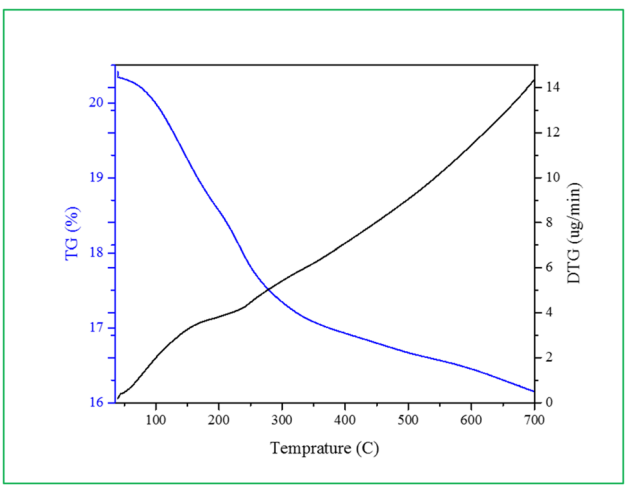

Fig. 8 TG-DTA analyses of Ca/4-MePy-IL@ZY-Fe_3O_4.

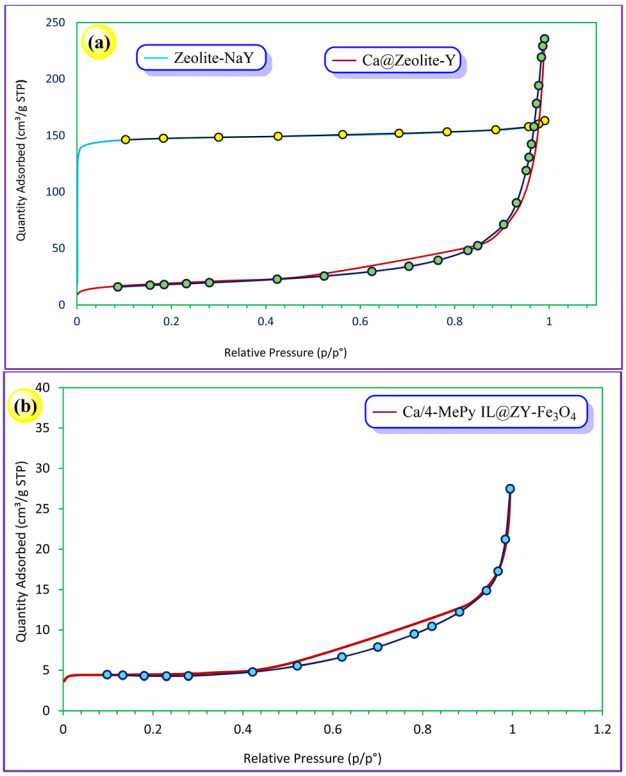

Fig. 9 N_2 adsorption/desorption isotherms of the zeolite–NaY, Ca@ZY (a) and its functionalized, Ca/4-MePy-IL@ZY-Fe_3O_4 (b).

mesoporous structure of zeolite–NaY has been preserved. As shown in Fig. 9b, according to the IUPAC classification, the N_2 adsorption–desorption isotherm of Ca/4-MePy-IL@ZY-Fe_3O_4 exhibits an H1-type hysteresis loop of type IV in the 0.42–0.88 $p/p°$ region, which is comparable to mesoporous materials. In addition, a quick check at the hysteresis type reveals that Ca/4-MePy-IL@ZY-Fe_3O_4 has slits (layer and layer with many pores) structure and that the initial nanostructure is kept after the functionalization.

Table 1 provides a summary of the structural information for zeolitic nanocomposites. Zeolite–NaY was measured for BET surface area (441.29 $m^2\ g^{-1}$) and pore size (2.21 nm). With the cation exchange of the Ca(II) ion inside the mesoporous of zeolite–NaY, the data of Ca@zeolite-Y in this table show that its surface area, pore volume, and maximum pore volume decreased. Compared to pure zeolite–NaY, Table 1 shows

Table 1 Porosimetery values for zeolite-Y and its functionalized

Samples	S_{BET}[a] ($m^2\ g^{-1}$)	V_{BJH}[b] ($cm^3\ g^{-1}$)	V_{Max}[c] ($cm^3\ g^{-1}$)	D_{Aap}[d] (nm)	W_{BJH}[e] (nm)
Zeolite–NaY	441.29	0.032	0.2282	2.2130	6.732
Ca@ZY	65.43	0.378	0.0288	9.4994	11.004
Ca/[$(MPy)^+Cl^-$]@ZY-Fe_3O_4	139.14	0.040	0.0692	7.0237	6.854

[a] Specific surface area. [b] Pore volume. [c] Maximum pore volume at $p/p° =$ 0.174699824 (estimated using the Horvath–Kawazoe method). [d] Adsorption average pore diameter ($4V/A$ by BET). [e] BJH Adsorption average pore width ($4V/A$).

Table 2 Optimization of 2-aminothiazole synthesis reaction conditions[a]

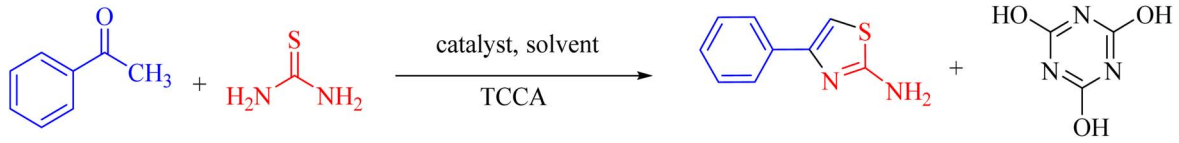

Entry	Catalyst loading (g), (wt/wt%)	Solvent	Temperature (°C)	Time (h)	Yield[b] (%)
1	—	EtOH	25, 50, 80	5	—
2	Ca/4-MePy-IL@ZY-Fe_3O_4 (5)	EtOH	25	2	10
3	Ca/4-MePy-IL@ZY-Fe_3O_4 (5)	EtOH	50	2	40
4	Ca/4-MePy-IL@ZY-Fe_3O_4 (5)	EtOH	80	1.5	75
5	Ca/4-MePy-IL@ZY-Fe_3O_4 (10)	EtOH	80	1.5	90
6	Ca/4-MePy-IL@ZY-Fe_3O_4 (15)	EtOH	80	1.3	90
7	Ca/4-MePy-IL@ZY-Fe_3O_4 (10)	H_2O : EtOH (1 : 1)	80	1.5	65
8	Ca/4-MePy-IL@ZY-Fe_3O_4 (10)	MeOH	80	1.5	91
9	Ca/4-MePy-IL@ZY-Fe_3O_4 (10)	DMSO	80	1.5	92
10	Ca/4-MePy-IL@ZY-Fe_3O_4 (10)	CH_3CN	80	1.5	60
11	Ca/4-MePy-IL@ZY-Fe_3O_4 (10)	CH_2Cl_2	40	1.5	75
12	Zeolite–NaY (10)	EtOH	80	1.5	30
13	Ca@zeolite-Y (10)	EtOH	80	1.5	50
14	Ca/4-MePy-IL@ZY (10)	EtOH	80	1.6	88
15	$AlCl_3$ (10)	EtOH	80	1.5	35
16	$CaCl_2$ (10)	EtOH	80	1.5	25
17	CaO (10)	EtOH	80	1.5	45

[a] Reaction conditions: acetophenone (1.5 mmol), thiourea (1.5 mmol), TCCA (0.5 mmol) and solvent (3 mL). [b] Isolated yield.

a decrease in BET surface area (139.14 $m^2\ g^{-1}$) and an increase in pore size (7.02 nm) for the functionalized nano-zeolite-Y. This decrease in BET surface area may be caused by the filling of the interconnected pores of the super cages with organic groups, which block the access to the inner surface of zeolite-Y. These findings demonstrate that ionic liquid groups have been grafted onto the pores of zeolite-Y.[39]

Table 3 Synthesis of 2-aminothiazole derivatives using Ca/4-MePy-IL@ZY-Fe_3O_4 catalyst[a]

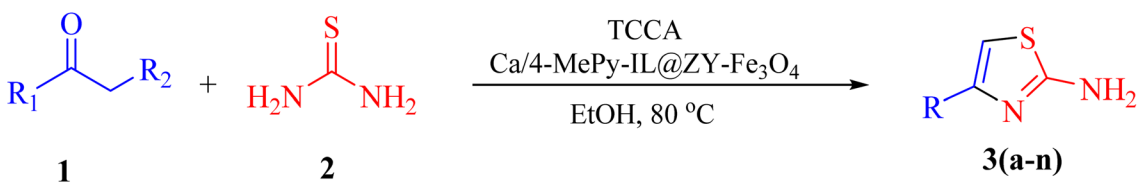

Entry	R_1 (R_2)	Product	MP (°C), (lit.)[c]	Time (h)	Yield[b] (%)
1	(H)	3a	152–153 (151–153)[40]	1.5	90
2	Br (H)	3b	182–184 (180–183)[40]	1.2	88

Table 3 (*Contd.*)

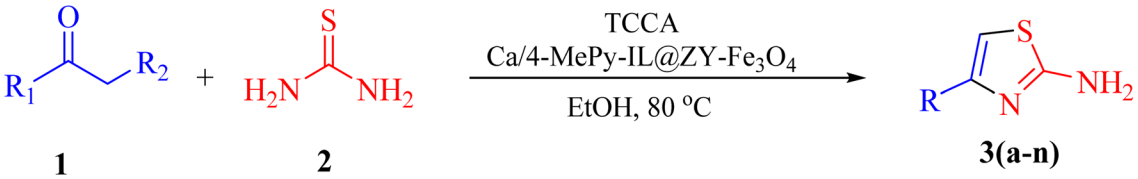

1 2 3(a-n)

Entry	R_1 (R_2)	Product	MP (°C), (lit.)[c]	Time (h)	Yield[b] (%)
3	CH_3 (CO–OEt)	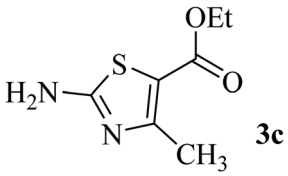 **3c**	175–177 (177–179)[40]	1.5	88
4	CH_3 (H)	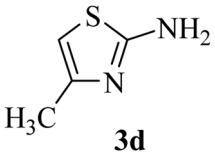 **3d**	55–56 (42–43)[41]	1	92
5	CH_3 ($CO–CH_3$)	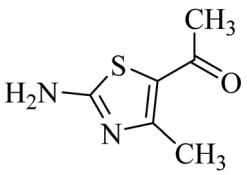 **3e**	215–217 (219–220)[40]	1.5	88
6	H (H)	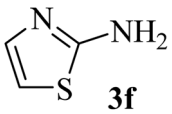 **3f**	93 (89–90)[40]	2	75
7	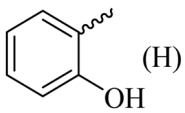	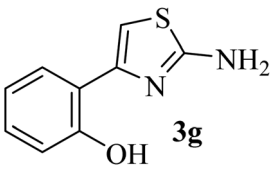 **3g**	136–138 (138–139)[40]	1.3	89
8	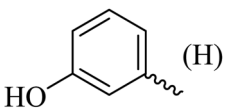	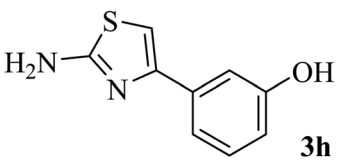 **3h**	138–140 (137–138)[8]	1.8	80
9	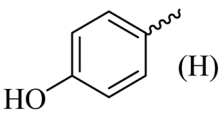	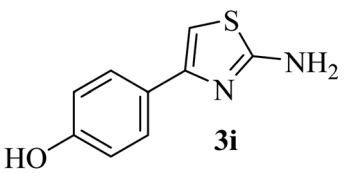 **3i**	198–200 (198–200)[40]	1.5	85
10	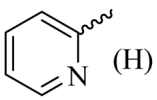	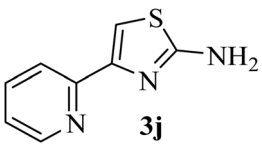 **3j**	154 (144–145)[41]	1.3	89

Table 3 (*Contd.*)

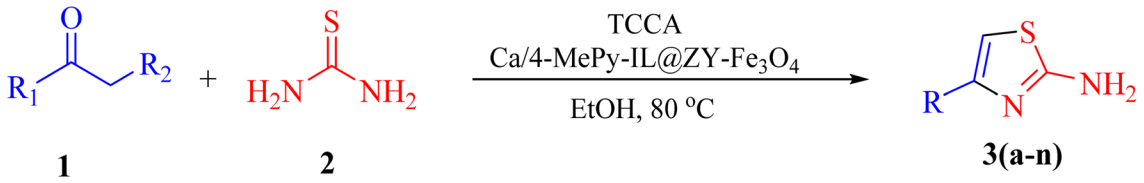

1 2 3(a-n)

Entry	R_1 (R_2)	Product	MP (°C), (lit.)[c]	Time (h)	Yield[b] (%)
11	(H)	3k	170–172 (175–177)[41]	1.5	82
12	(H)	3l	261 (272–275)[42]	1.5	89
13		3m	192 (205–207)[43]	1.3	90
14		3n	214 (175)[44]	2	75

[a] Reaction conditions: methylcarbonyl (1.5 mmol), thiourea (1 mmol), TCCA (0.5 mmol), catalyst (10% wt/wt) and EtOH (3 mL) 80 °C. [b] Isolated yield. [c] Melting points are reported in the literature.

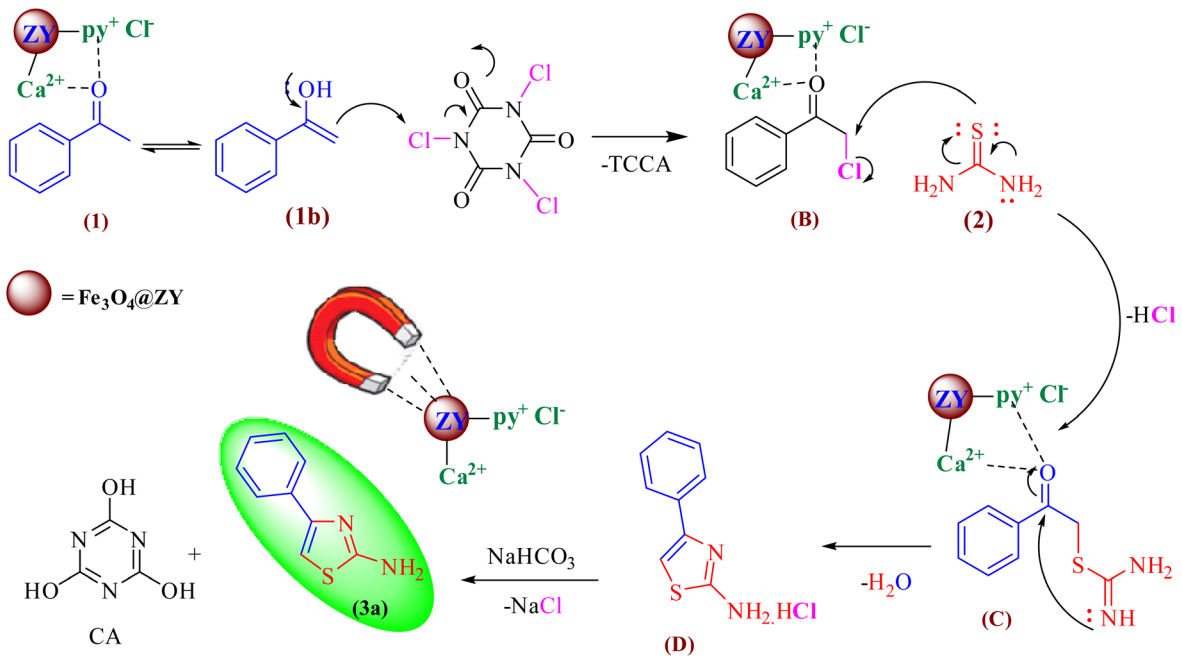

Scheme 3 The proposed mechanism for the preparation of 2-aminothiazoles using Ca/4-MePy-IL@ZY-Fe_3O_4 catalyst.

3.2. Catalytic activity of Ca/4-MePy-IL@ZY-Fe_3O_4

For the production of 2-aminothiazoles the catalytic activity of generated Ca/4-MePy-IL@ZY-Fe_3O_4 was evaluated. In order to establish the ideal conditions, acetophenone, thiourea, and TCCA were chosen as the required substrates for the model reaction (Table 2). To improve the reaction conditions, the amount of nanocatalyst, the influence of temperature, and the solvent were all investigated. Control experiments show that no reaction occurs without the presence of the catalyst (Table 2, entry 1). However, the yield of the product was increased by increasing the amount of catalyst. The optimal amount of Ca/4-MePy-IL@ZY-Fe_3O_4 was discovered to be 10% wt/wt at 80 °C and the solvent EtOH was regarded as a suitable solvent (entry 5). However, at the same time period, the reaction yield was not improved by adding additional Ca/4-MePy-IL@ZY-Fe_3O_4 to the mixture (entry 6). Other solvents failed to enhance this catalytic process (entries 7–11). Also present during this reaction were zeolite–NaY, Ca@zeolite-Y, and Ca/4-MePy-IL@ZY. The products' respective yields of 30%, 60%, and 88% (entries 12 to 14) demonstrate the highest performance when the nanocatalyst is utilized in several processes. Also, looking at entries 12–17 in Table 2 and the experiences gained in this field, it can be assumed that the presence of a catalyst with higher basicity improves the conditions of this type of reactions and it seems that the ionic liquid moiety of 4-methylpyridinium chloride (basic) grafted on the magnetic zeolite surface, play a more important and effective role in the one-pot synthesis of 2-aminothiazole.

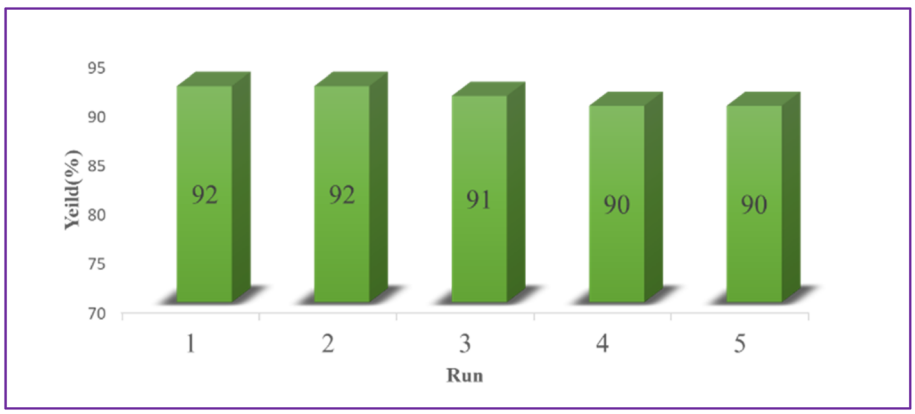

Fig. 10 Reusability of Ca/4-MePy-IL@ZY-Fe_3O_4 using the model reaction.

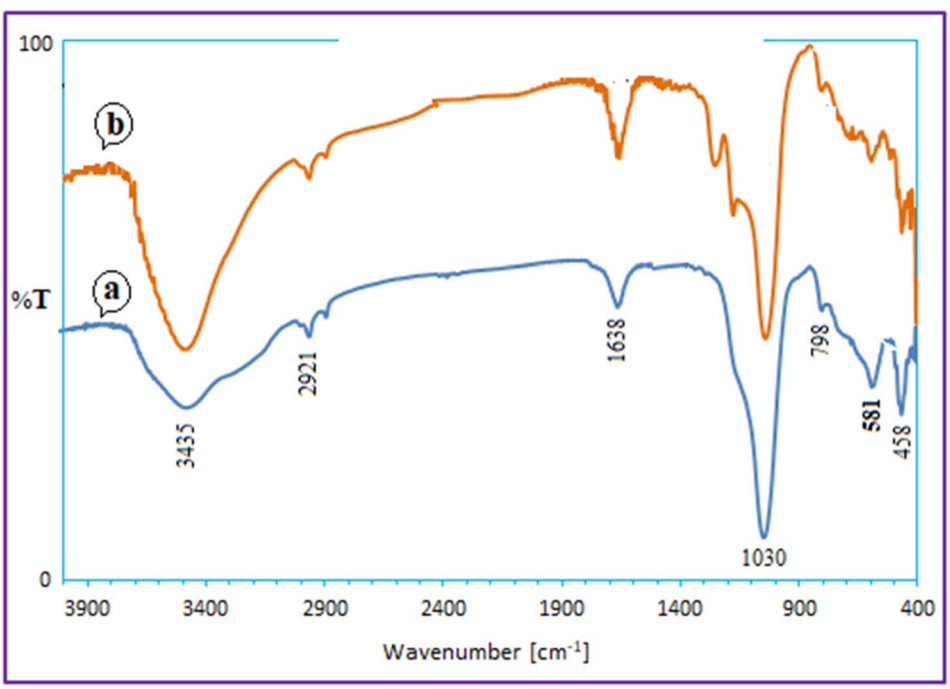

Fig. 11 FT-IR spectrum of recovered Ca/4-MePy-IL@ZY-Fe_3O_4 (a) after the 5 cycle and the fresh nanocatalyst (b).

To demonstrate the flexibility and productivity of this new approach for the production of 2-aminothiazoles, a large number of methylcarbonyls containing electron-donating or electron-withdrawing groups were mixed with thiourea in EtOH at 80 °C using Ca/4-MePy-IL@ZY-Fe_3O_4 as a catalyst. As shown in Table 3, the procedure was quite effective, and the kind of substituent had little impact on the reaction yields. The heterogeneous nanohybrids' multifunctionality appears to speed up the rate of response. Selectivity also contributes significantly to the creation of other organic molecules.

In Scheme 3, the suggested mechanism for the synthesis of 2-aminothiazoles is shown. Through a Lewis acid or Lewis basic catalyzed method, the Ca/4-MePy-IL@ZY-Fe_3O_4 nanohybrids support this reaction. First, the methyl carbonyl group is activated through the acidic sites (Lewis or Brønsted acid) of the nanocatalyst and with a nucleophilic attack on the chlorine electrophilic center in TCCA leads to the formation of chloromethylene carbonyl benzene intermediate (**B**). Next, with the nucleophilic attack of the thiol group (thiourea, **1**) to the chloromethylene center, intermediate (**C**) is obtained. Immediately, through an intramolecular nucleophilic condensation reaction of *N*-imine to the center of the carbonyl group activated by the catalyst, a thiazole salt (**D**) is formed. Finally, by neutralizing the reaction mixture with sodium bicarbonate solution, 2-aminothiazole product is obtained.

3.3. Catalyst recyclability

Using the model reaction under the idealized circumstances, it was determined if the heterogeneous catalyst Ca/4-MePy-IL@ZY-Fe_3O_4 was reusable. To do this, the catalytic nanohybrid was isolated for use in this purpose by an external magnet once the reaction was complete. The remaining nanocatalyst was repeatedly washed with water and ethanol before being dried at 50 °C. The catalyst was successfully activated for the production of 2-aminothiazoles after five cycles, as observed (Fig. 10).

The FT-IR spectroscopy also verified the fundamental structure of the reused catalyst. The FT-IR spectra of the recovered and fresh zeolitic catalysts, as shown in Fig. 11, essentially do not differ from one another.

The FT-IR spectroscopy also verified the fundamental structure of the reused catalyst. The FT-IR spectra of the recovered and fresh zeolitic catalysts, as shown in Fig. 11, essentially do not differ from one another.

4. Conclusions

In this study, we synthesized and investigated Ca@zeolite-Y/Fe_3O_4 supported 4-methylpyridinium ionic liquid as a new, effective, magnetically and multi-functional nanocatalyst for the preparation of 2-aminothiazoles under environmentally friendly conditions. The presence of Lewis acid (Ca^{2+}) and basic ionic liquid (4-methylpyridinium chloride) sites on a magnetically nanoporous solid surface (multi-functional) is one of the apparent advantages of this nanocatalyst. The current approach also has certain benefits, including excellent product yields, extraordinary speed, the use of nanotechnology in the catalytic process, the catalyst's reusability, easy separation of the nanocatalyst from the reaction medium by an external magnet, cheap cost, and its non-toxic nature.

Data availability

The spectral data which could be supported our findings are available as ESI† attached to this article.

Conflicts of interest

The authors declare that they have no interest to influence the work reported in this paper.

Acknowledgements

We are thankful to the Payame Noor University for the partial support of this work.

References

1 S. Ghaemmaghami, B. C. May, A. R. Renslo and S. B. Prusiner, Discovery of 2-aminothiazoles as potent antiprion compounds, *J. virol.*, 2010, **84**, 3408–3412.
2 S. Imtiaz and S. Banoo, α-Aminoazoles/azines: key reaction partners for multicomponent reactions, *RSC Adv.*, 2021, **11**, 11083–11165.
3 L. M. Frija, A. J. Pombeiro and M. N. Kopylovich, Coordination chemistry of thiazoles, isothiazoles and thiadiazoles, *Coord. Chem. Rev.*, 2016, **308**, 32–55.
4 R. Patil, J. Chavan and A. Beldar, Synthesis of aminothiazoles: Polymer-supported approaches, *RSC Adv.*, 2017, **7**, 23765–23778.
5 A. Gahtori, A. Kumar, P. Kothiyal and P. Gahtori, Facile and efficient preparation of hybrid phenylthiazolyl-1,3,5-triazines and their antidepressant-like effect in mice, *Tetrahedron Lett.*, 2014, **55**, 4987–4990.
6 A. Hantzsch and J. Weber, Ueber verbindungen des thiazols (pyridins der thiophenreihe), *Ber. Dtsch. Chem. Ges.*, 1887, **20**, 3118–3132.
7 B. Dziuk, J. B. Kyzioł, J. Zaleski, K. Ejsmont and B. Zarychta, Synthesis of 2-Aminothiazole Derivatives in Easy Two-Step, One-Pot Reaction, *J. Heterocycl. Chem.*, 2018, **55**, 763–768.
8 M. Kalhor and Z. Zarnegar, 1-Methylimidazolium ionic liquid supported on Ni@zeolite-Y: fabrication and performance as a novel multi-functional nanocatalyst for one-pot synthesis of 2-aminothiazoles and 2-aryl benzimidazoles, *Res. Chem. Intermed.*, 2022, **48**, 519–540.
9 I. I. Roslan, K. H. Ng, M. A. Gondal, C. Basheer, M. A. Dastageer, S. Jaenicke and G. K. Chuah, Visible Light-Mediated Coupling of Thioureas and 1, 3-Dicarbonyls: Towards a Leaving Group-Free Synthesis of Aminothiazoles, *Adv. Synth. Catal.*, 2018, **360**, 1584–1589.
10 J. Safari and M. Sadeghi, Nanostarch: a novel and green catalyst for synthesis of 2-aminothiazoles, *Monatsh. Chem.*, 2017, **148**, 745–749.

11 J. Safari, Z. Shokrani and Z. Zarnegar, Asparagine as a Green Organocatalyst for the Synthesis of 2-Aminothiazoles, *Polycyclic Aromat. Compd.*, 2020, **40**, 1105–1111.
12 G. Meng, M. Wang, A. Zheng, J. Dou and Z. Guo, Efficient one-pot synthesis of ethyl 2-substitued-4-methylthiazole-5-carboxylates, *Green Chem. Lett. Rev.*, 2014, **7**, 46–49.
13 M. Narender, M. S. Reddy, V. P. Kumar, B. Srinivas, R. Sridhar, Y. V. D. Nageswar and K. R. Rao, Aqueous-phase one-pot synthesis of 2-aminothiazole-or 2-aminoselenazole-5-carboxylates from β-keto esters, thiourea or selenourea, and n-bromo-succinimide under supramolecular catalysis, *Synthesis*, 2007, **22**, 3469–3472.
14 M. Sadeghi, J. Safari and Z. Zarnegar, Synthesis of 2-aminothiazoles from methylcarbonyl compounds using a Fe_3O_4 nanoparticle-*N*-halo reagent catalytic system, *RSC Adv.*, 2016, **6**, 64749–64755.
15 (*a*) H. Huang, Z. Qu, X. Ji and G. Deng, Three-component bis-heterocycliation for synthesis of 2-aminobenzo[4,5]thieno[3,2-*d*]thiazoles, *Org. Chem. Front.*, 2019, **6**, 1146–1150; (*b*) S.-F. Yang, P. Li, Z.-L. Fang, S. Liang, H.-Y. Tian, B.-G. Sun, K. Xu and C.-C. Zeng, A one-pot electrochemical synthesis of 2-aminothiazoles from active methylene ketones and thioureas mediated by NH4I, *Beilstein J. Org. Chem.*, 2022, **18**, 1249–1255.
16 K. Banert and J. Seifert, Steric hindrance classified: treatment of isothiocyanatoallene with secondary amines bearing bulky substituents to generate 2-aminothiazoles, *Org. Chem. Front.*, 2019, **6**, 3517–3522.
17 V. S. de Andrade and M. C. de Mattos, One-pot synthesis of 4-aryl-2-aminothiazoles from styrenes and thioureas promoted by tribromoisocyanuric acid, *Tetrahedron Lett.*, 2020, **61**, 152164.
18 S. D. Tozetti, L. S. D. Almeida, P. M. Esteves and M. Mattos, Trihaloisocyanuric acids/NaX: an environmental friendly system for vicinal dihalogenation of alkenes without using molecular halogen, *J. Braz. Chem. Soc.*, 2007, **18**, 675–677.
19 L. S de Almeida, P. M Esteves and M. CS de Mattos, Tribromoisocyanuric acid: a green and versatile reagent, *Curr. Green Chem.*, 2014, **1**, 94–107.
20 S. Gaspa, M. Carraro, L. Pisano, A. Porcheddu and L. De Luca, Trichloroisocyanuric acid: a versatile and efficient chlorinating and oxidizing reagent, *Eur. J. Org. Chem.*, 2019, **2019**, 3544–3552.
21 (*a*) I. Saidalimu, Y. Liang, K. Niina, K. Tanagawa, N. Saito and N. Shibata, Synthesis of aryl and heteroaryl tetrafluoro-λ6-sulfanyl chlorides from diaryl disulfides using trichloroisocyanuric acid and potassium fluoride, *Org. Chem. Front.*, 2019, **6**, 1157–1161; (*b*) G. F Mendonca and M. CS de Mattos, Green chlorination of organic compounds using trichloroisocyanuric acid (TCCA), *Curr. Org. Syn.*, 2013, **10**, 820–836.
22 M. M. Heravi, B. Heidari, V. Zadsirjan and L. Mohammadi, Applications of Cu (0) encapsulated nanocatalysts as superior catalytic systems in Cu-catalyzed organic transformations, *RSC Adv.*, 2020, **10**, 24893–24940.
23 C. G. Lima, N. M. Moreira, M. W. Paixao and A. G. Correa, Heterogenous green catalysis: Application of zeolites on multicomponent reactions, *Curr. Opin. Green Sustain. Chem.*, 2019, **15**, 7–12.
24 W. N. van der Graaff, E. A. Pidko and E. J. Hensen, in *Zeolites in Sustainable Chemistry*, Springer, 2016, pp. 347–372.
25 J. Liang, Z. Liang, R. Zou and Y. Zhao, Heterogeneous catalysis in zeolites, mesoporous silica, and metal–organic frameworks, *Adv. Mater.*, 2017, **29**, 1701139.
26 N. Ndiege, R. Raidoo, M. K. Schultz and S. Larsen, Preparation of a versatile bifunctional zeolite for targeted imaging applications, *Langmuir*, 2011, **27**, 2904–2909.
27 D. Jagadeesan, Multifunctional nanocatalysts for tandem reactions: A leap toward sustainability, *Appl. Catal., A*, 2016, **511**, 59–77.
28 M. Kalhor, Z. Orouji and M. Khalaj, 4-Methylpyridinium chloride ionic liquid grafted on Mn@ zeolite-Y: Design, fabrication and performance as a novel multi-functional nanocatalyst in the four-component synthesis of pyrazolophthalazine-diones, *Microporous Mesoporous Mater.*, 2022, **329**, 111498.
29 C. Srilakshmi, R. Saraf and C. Shivakumara, Structural studies of multifunctional SrTiO3 nanocatalyst synthesized by microwave and oxalate methods: its catalytic application for condensation, hydrogenation, and amination reactions, *ACS Omega*, 2018, **3**, 10503–10512.
30 K. Arya, D. S. Rawat and H. Sasai, Zeolite supported Brønsted-acid ionic liquids: an eco approach for synthesis of spiro [indole-pyrido [3, 2-e] thiazine] in water under ultrasonication, *Green Chem.*, 2012, **14**, 1956–1963.
31 A. Ehsani, M. Moftakhar and M. Kalhor, Mesoporous ionic liquid functionalized nanozeolite: Synthesis and high efficient material to improving pseudocapacitance performance of conductive polymer, *J. Energy Storage*, 2022, **55**, 105489.
32 A. A. Raheem, P. Thangasamy, M. Sathish and C. Praveen, Supercritical water assisted preparation of recyclable gold nanoparticles and their catalytic utility in cross-coupling reactions under sustainable conditions, *Nanoscale Adv.*, 2019, **1**, 3177–3191.
33 M. Nasrollahzadeh, M. Ghasemzadeh, H. Gharoubi and Z. Nezafat, Progresses in polysaccharide and lignin-based ionic liquids: Catalytic applications and environmental remediation, *J. Mol. Liq.*, 2021, **342**, 117559.
34 (*a*) S. Sowmiah, J. M. S. S. Esperança, L. P. N. Rebelo and C. A. M. Afonso, Pyridinium salts: from synthesis to reactivity and applications, *Org. Chem. Front.*, 2018, **5**, 453–493; (*b*) R. L. Vekariya, A review of ionic liquids: Applications towards catalytic organic transformations, *J. Mol. Liq.*, 2017, **227**, 44–60.
35 M. Kalhor and Z. Zarnegar, Fe_3O_4/SO_3H@ zeolite-Y as a novel multi-functional and magnetic nanocatalyst for clean and soft synthesis of imidazole and perimidine derivatives, *RSC Adv.*, 2019, **9**, 19333–19346.
36 (*a*) M. Phanindrudu, D. K. Tiwari, B. Sridhar, P. R. Likhar and D. K. Tiwari, Magnetically separable nano-copper catalyzed unprecedented stereoselective synthesis of E-vinyl sulfones from tosylmethyl isocyanide and alkynes: TosMIC as a source of the sulfonyl group, *Org. Chem.*

Front., 2016, **3**, 795–798; (*b*) L. M. Rossi, N. J. Costa, F. P. Silva and R. Wojcieszak, Magnetic nanomaterials in catalysis: advanced catalysts for magnetic separation and beyond, *Green Chem.*, 2014, **16**, 2906–2933.

37 P. S. Endang, A. R. Rahadian, T. I. M. Ulva, R. W. Alvin, M. I. Rendy and N. Widiastuti, The MnO_2/zeolite Nay catalyzed oxidation of co emission in catalytic converter system, *Mater. Sci. Forum*, 2019, **964**, 199–208.

38 S. M.-G. Yek, M. Nasrollahzadeh, D. Azarifar, A. Rostami-Vartooni, M. Ghaemi and M. Shokouhimehr, Grafting Schiff base Cu(II) complex on magnetic graphene oxide as an efficient recyclable catalyst for the synthesis of 4*H*-pyrano [2,3-b] pyridine-3-carboxylate derivatives, *Mater. Chem. Phys.*, 2022, **284**, 126053.

39 P. Li, Y. Wang, H. Li and G. Calzaferri, Luminescence enhancement after adding stoppers to europium (III) nanozeolite L, *Angew. Chem., Int. Ed.*, 2014, **53**, 2904–2909.

40 J. Safari, Z. Abedi-Jazini, Z. Zarnegar and M. Sadeghi, Nanochitosan: A biopolymer catalytic system for the synthesis of 2-aminothiazoles, *Catal. Commun.*, 2016, **77**, 108–112.

41 P. Kakati, P. Singh, P. Yadav and S. K. Awasthi, Aiding the versatility of simple ammonium ionic liquids by the synthesis of bioactive 1, 2, 3, 4-tetrahydropyrimidine, 2-aminothiazole and quinazolinone derivatives, *New J. Chem.*, 2021, **45**, 6724–6738.

42 S. Ma, L. Wang, B. Ouyang, M. Fan, J. Qi and L. Yao, Design, synthesis and biological evaluation of 4-aryl-5-aminoalkyl-thiazole-2-amines derivatives as ROCK II inhibitors, *Bioorg. Med. Chem.*, 2020, **28**, 115683.

43 A. V. Galochkina, R. K. Bollikanda, V. V. Zarubaev, D. G. Tentler, I. N. Lavrenteva, A. V. Slita, N. Chirra and S. Kantevari, Synthesis of novel derivatives of 7, 8-dihydro-6H-imidazo [2,1-b][1,3] benzothiazol-5-one and their virus-inhibiting activity against influenza A virus, *Arch. Pharm.*, 2019, **352**, 1800225.

44 P. Ferraboschi, S. Ciceri, P. Ciuffreda, M. De Mieri, D. Romano and P. Grisenti, Baker's yeast catalyzed preparation of a new enantiomerically pure synthon of (S)-pramipexole and its enantiomer (dexpramipexole), *Tetrahedron: Asymmetry*, 2014, **25**, 1239–1245.